

## D2.2

# Test Methodology Report

June 2025

## Document Information

| Name  | Organisation               | Contribution  |
|---|----------------------------|---|
| Milan Lovric, Pradyot Pendyala, Rufus Eade, Hetian Wang, Valentina Donzella | WMG, University of Warwick | Report layout, introduction, sensor noise factor testing in the laboratory, conclusions |

## Abbreviations and Acronyms

|       |                                   |
|-------|-----------------------------------|
| ADAS  | Advanced Driver Assistance System |
| ADS   | Automated Driving System          |
| DSLR  | Digital Single-Lens Reflex Camera |
| FOV   | Field of View                     |
| LiDAR | Light Detection and Ranging       |
| MEMS  | Micro Electro-Mechanical Systems  |
| PPE   | Personal Protective Equipment     |
| ROS   | Robot Operating System            |
| TOF   | Time of Flight                    |
| WMG   | Warwick Manufacturing Group       |

# Contents

|  |    |
|--|----|
| Document Information .....   | 2  |
| Abbreviations and Acronyms .....   | 3  |
| Contents .....   | 4  |
| 1. Introduction .....  | 6  |
| 2. LiDAR Noise Factor Testing in the Lab.....  | 7  |
| 2.1. Equipment.....  | 7  |
| ▪ LiDAR Sensors .....  | 7  |
| ▪ Noise Factor Materials and Equipment .....   | 7  |
| ▪ Cleaning Materials and Method .....  | 8  |
| ▪ PPE .....  | 9  |
| 2.2. Experimental Setup.....   | 10 |
| 2.3. Experimental Procedure .....  | 11 |
| ▪ Baseline LiDAR Readings.....   | 11 |
| ▪ Photos of the Active Face of LiDAR Sensor.....                                     | 11 |
| 2.4. Study A: Clear Water Droplets.....  | 12 |
| 2.5. Study B: Muddy Water Droplets.....  | 13 |
| 2.6. Quantifying the Percentage of LiDAR's Active Face Affected by the Noise Factors | 14 |
| ▪ Imbinarise Image Processing Method .....   | 14 |
| ▪ Canny Edge Detection.....  | 15 |
| ▪ Combining Morphological Operations with Canny Edge Detection and Imbinarise        | 15 |
| ▪ Processing the Images from the Laboratory Experiments .....                        | 16 |
| ▪ Quantifying the impact on LiDAR point cloud .....                                  | 17 |
| 2.7. Results.....  | 18 |
| ▪ Clear Water Droplets .....   | 18 |
| ▪ Muddy Water Droplets.....  | 21 |
| .....  | 22 |
| 3. Conclusions .....   | 25 |
| Appendix I – Datasets.....   | 27 |
| 3.1. Water Droplets .....  | 28 |

|      |                           |    |
|------|---------------------------|----|
| ▪    | LiDAR A.....              | 28 |
| ▪    | LiDAR B.....              | 29 |
| ▪    | LiDAR C.....              | 31 |
| 3.2. | Muddy Water Droplets..... | 34 |
| ▪    | LiDAR A.....              | 34 |
| ▪    | LiDAR B.....              | 36 |
| ▪    | LiDAR C.....              | 37 |

# 1. Introduction

The automotive industry is currently focused on development of Advanced Driver Assistance Systems (ADAS) and lower levels of automation. Nevertheless, recent years have also seen a growing interest in higher levels of vehicle autonomy enabled by Automated Driving Systems (ADS). A requirement that has attracted significant scrutineering to make these varying levels of autonomy possible is safety. Safety is of paramount importance to all automotive applications, especially when driving is based on input data from perception sensors, which may degrade due to presence of numerous noise factors including those of environmental origin.

LiDAR (Light Detection and Ranging) sensors have emerged as a promising technology, and they are presently under extensive research for automotive applications owing to their high spatial resolution, accurate depth perception, and the ability to operate in low-light conditions. Most LiDAR sensors are time of flight (TOF) sensors which emit pulsed light waves – typically in the near-infrared range – into the surrounding environment. These laser beams then bounce off surrounding objects and return to the sensor. The time required for the pulses to return enables the calculation of distances to the surrounding objects. This data is then used to build a 3D point cloud which contains spatial coordinates of objects and additional attributes such as reflection intensity.

However, this technology is also susceptible to environmental noise factors, such as rain precipitation or a spray of muddy water pooled on the road surface, which could cover the active face of the sensor and potentially obstruct pulses from being transmitted or received. This then raises significant safety concerns, as it may result in data degradation or complete signal loss. While there have been research papers investigating these effects through simulations, direct empirical investigations of these factors remain relatively scarce.

This report systematically examines the effects of environmental noise factors, specifically LiDAR occlusion with clear and muddy water droplets, through controlled laboratory experimentation involving direct application to the active surfaces of tested LiDAR devices. The investigation encompasses comparative analysis of state-of-the-art automotive LiDAR systems, with particular emphasis on quantifying the degradation of point cloud data quality under recreated adverse conditions. Through examination of these interactions, this report contributes to a better understanding of how sensors occlusion phenomena could potentially impact vehicular safety.

## 2. LiDAR Noise Factor Testing in the Lab

### 2.1. Equipment

#### ■ LiDAR Sensors

The experiments we conducted in the laboratory investigated the impact of noise factors on three LiDAR sensors, listed in Table 1. The selected sensors are based on solid-state technology and have comparable Field of Views (FOV), which facilitated meaningful analysis and comparison across the sensors. Two of the LiDARs operate at 905 nm wavelength and one of the sensors at 1550 nm, which allowed for testing of wavelength-dependent susceptibility to noise factors.

LiDAR A and LiDAR B have flat active surfaces whereas LiDAR C has a convex, bow-front shaped active face. This geometric differentiation might be relevant in case the applied noise factors behaved differently on flat and curved surfaces. Furthermore, LiDAR B was the largest device of the three and also had the largest active face. LiDAR C on the other hand constituted the most compact device with correspondingly reduced active face dimensions.

Table 1: List of LiDARs used in the experiments.

| Sensor Model | Sensing Tech.           | Wave-length [nm] | Range [m] | Range Precision [cm] | Points Rate [pts/s]                  | FOV  | Blind Spot [m] | Mass [g] | Ingress Protection Classification |
|--------------|-------------------------|------------------|-----------|----------------------|--------------------------------------|--|----------------|----------|-----------------------------------|
| LiDAR A      | Non-repetitive scanning | 905              | 150       | $\pm 3$              | 452,000                              | 120° (Horizontal)<br>25° (Vertical)                                | <0.5           | 1120     | IP67                              |
| LiDAR B      | Semi-solid state        | 1550             | 250       | $\pm 5$              | 900,000                              | 120° / 40°<br>(Horizontal / ROI)<br>25° / 4.8°<br>(Vertical / ROI) | <1.5           | 1700     | IP67, IP69K                       |
| LiDAR C      | MEMS solid-state LiDAR  | 905              | 180       | $\pm 5$              | 787,500 (Single)<br>1,575,000 (Dual) | 120° (Horizontal)<br>25° (Vertical)<br>$\pm 0.2^\circ$             | <0.5           | 690      | IP67, IP6K9K                      |

#### ■ Noise Factor Materials and Equipment

Figure 1 shows the equipment used for the preparation and application of noise factors. The bottles were used for the volumetric measurement of water when preparing for the muddy water droplets experiments. The high-precision weighing scale was used to measure out the clay powder to formulate muddy droplets of different concentration and viscosity. The petri dish was used to mix clay and water for the mud occlusions experiments. The VITLAB 400 ml spray bottle, equipped with an adjustable red nozzle, provided controlled dispersion of liquids

ranging from fine mist to directed streams, enabling application of both clear and muddy water droplets onto active LiDAR surfaces. Standard tap water served as the aqueous medium, while the clay powder selected for use in these experiments was Bentonite 285234 from Sigma Alderich. This substance was selected for its non-hazardous properties and straightforward disposal protocols, as noted in its chemical data sheet.

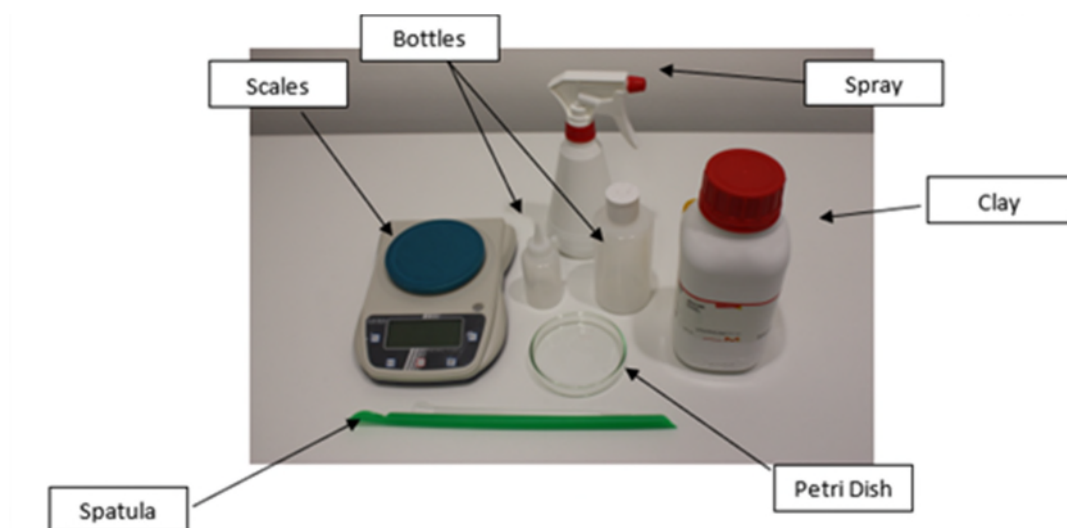


Figure 1: Noise factor tools and materials.

### ■ Cleaning Materials and Method

Cleaning the sensors after each run was a critical aspect of the experimental protocol, ensuring all the occlusions are removed before completing another run of experiments, while also safeguarding against sensor damage. Furthermore, it was important to avoid introducing new noise factors into the experiment such as lint from the wipes used. The manufacturers recommend implementing pressurised air into the cleaning process to prevent damage to the sensor's active face.

To clean the sensors safely and effectively, Kimwipes were used. These disposable wipes can remove liquid, dust, and small particles without scratching the lens and are traditionally used to clean instruments in laboratories. This was sufficient for wiping the active face clean after it was used for a clear water droplet experiment. However, when muddy water was applied, the cleaning process became more elaborate. If the droplets had dried, which occurred when the sensor was in operation for extended periods of time and became hot, some water was sprayed onto the active face to loosen up the dried droplets. Bio-Pure pre-moistened alcohol wipes were then used to remove the muddy droplets from the sensor face. This, however, would often leave lint on the sensor face, which if directly wiped may have scratched the face, hence a second spray of water was reapplied. The sensor was then wiped with Kimwipes and allowed to dry.



After each cleaning process, the sensor face was visually inspected for presence of any noise factors such as lint or streaks from the droplets that were not removed properly. The point cloud was further visually inspected to see if the LiDAR output returned close to the baseline readings taken in the previous run.



Figure 2: Cleaning paper wipes.



Figure 3: Cleaning wet wipes.

#### ■ PPE

All three LiDAR units conformed to the Class 1 laser safety standard, rendering them eye-safe under normal operating conditions. However, since LiDARs were approached very closely when applying noise factors and cleaning, Thorlabs LG2 Laser Safety Glasses (870 – 1600 nm, OD = 4+) were worn during the experimentation, out of an abundance of caution. This also provided protection against clay powder ingress, thus preventing any harm or irritation. Finally, nitrile gloves were worn when handling the clay powder as a safety precaution.



Figure 4: Laser safety glasses.



Figure 5: Gloves.

## 2.2. Experimental Setup

As shown in Figure 6, traffic cones and calibrated targets were positioned at one end of the room, with the LiDAR sensor stationed on the opposite side of the room and oriented towards the centre of the target array. This configuration did not need to be changed as all three sensors under investigation have the same FOV.

The experimental setup incorporated one 20x20 cm and one 50x50 cm, 90%-reflectivity calibrated target sourced from Zenith Lite. These are built from 1 mm or 2 mm proprietary polymer diffuser bonded to a 10-15 mm aluminium honeycomb structured plate with a high-performance adhesive. Complementing these reflectance boards, three traffic cones were strategically positioned to provide insight into the varied effect across the FOV when a noise factor is applied.

As depicted in Figure 6, the experimental chamber featured white interior walls, supplemented by a white curtain on the left and white blinds on the right. The blinds were fully closed to block any external illumination. Artificial room lighting was maintained at maximum intensity to ensure optimal visibility for the researchers, while also establishing consistent ambient lighting conditions across the experimental runs. Using a JETI Spectral 1511 spectroradiometer, eleven luminance measurements were taken at distinct locations within the room. The brightest region registered 186.8 cd/m<sup>2</sup> and the lowest 115.8 cd/m<sup>2</sup>. The average luminance in the laboratory was 156.2091 cd/m<sup>2</sup> with a standard deviation of 24.4192 cd/m<sup>2</sup>.



Figure 6: WMG Perception Sensors Testing Laboratory.

## 2.3. Experimental Procedure

### ■ Baseline LiDAR Readings

Prior to collecting data for the experimental runs, a baseline measurement was necessary. This was accomplished by placing the sensor in the correct position and keeping it stationary, followed by recording a 10-second ROS bag without any water or mud occlusion. Obtaining these measurements without noise factors allowed for comparisons with subsequent readings when noise factors were applied. If the LiDAR was accidentally moved, a new baseline had to be recorded to ensure accurate metric assessment and valid comparisons.

### ■ Photos of the Active Face of LiDAR Sensor

To quantify the amount of water and mud applied to the sensor, a DSLR camera mounted at a fixed height and position on a tripod was used to capture the images of the LiDAR's front face. These images were then further processed – as explained in the methodology section – to determine the percentage of the sensor's active surface area affected by the noise factors. The tripod position was marked with tape (as seen in Figure 7) because the tripod had to be moved whenever a LiDAR ROS bag was being collected. This ensured the photos of the sensor front face were consistent in terms of positioning, lighting, and height whenever the noise factors were applied. Furthermore, all photos were captured with flash to help highlight the droplets for improved algorithmic detection during image processing.



Figure 7: Camera setup for taking photos of the LiDAR front face.

## 2.4. Study A: Clear Water Droplets

To collect ROS bags containing LiDAR point cloud data, the following method was followed:

First, a baseline recording was taken as outlined previously.

Next, a spray bottle was filled with at least 200 ml of water. The sensor was then sprayed once from a consistent level relative to the sensor face, and a photo of the sensor' active face was taken with the DSLR camera.

Subsequently, a ROS bag of the LiDAR data with noise factor applied was recorded. This process was repeated two more times without wiping the sensor, with the sensor being sprayed twice (in total) on the second run and three times (in total) on the third run. If the sensor moved due to any circumstances, a new baseline was taken prior to continuation.

This progressive approach was done to gradually increase droplet coverage of the active face. Finally, the sensor was wiped clean as directed before. This process was then repeated six more times giving a total of seven sets of data. This procedure is outlined in Figure 8.

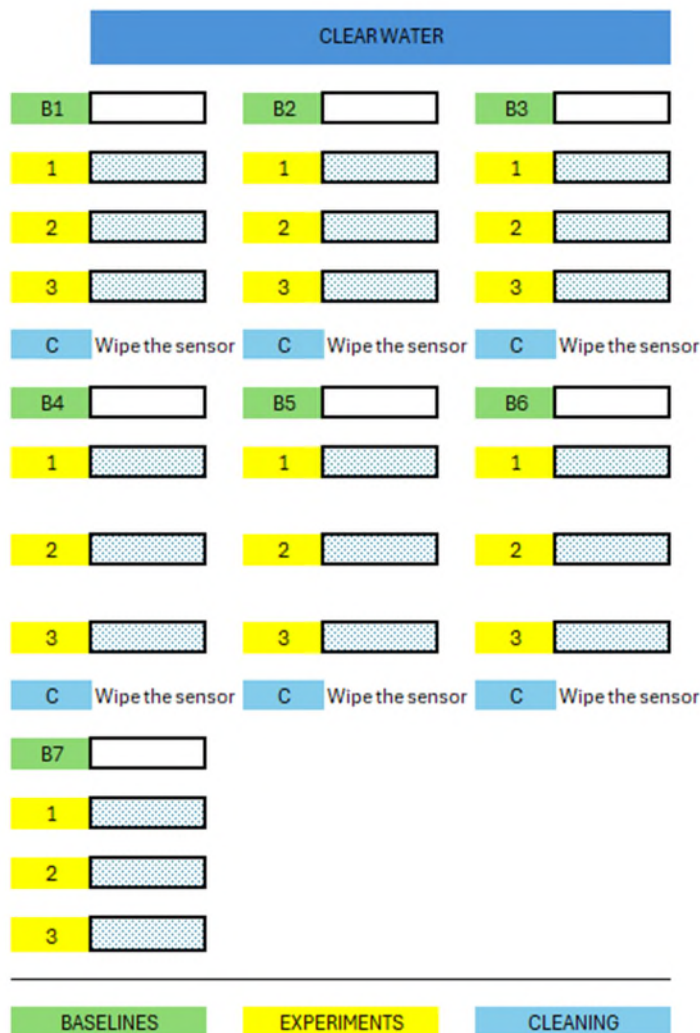


Figure 8: Experimental design for clear water droplets study.



## 2.5. Study B: Muddy Water Droplets

To collect ROS bags containing LiDAR point cloud data, the following method was followed:

First, a baseline recording was taken as outlined previously.

Next, a spray bottle was filled with 100 ml of water. One scoop or 1.48 g of the clay powder was added to the spray bottle using the spatula with a measuring spoon on one end, and the bottle was shaken vigorously to mix well. The sensor was then sprayed once from a consistent level relative to the sensor's active face, and a photo of the active face was taken with the DSLR camera.

Afterwards, a ROS bag of the LiDAR data with noise factor applied was recorded. This process was repeated two more times without wiping the sensor, with the sensor being sprayed twice on the second run and three times on the third run. If the sensor moved due to any circumstances, a new baseline was taken before continuing.

This was done to gradually increase how much of the active face was covered with muddy water droplets. After three experimental runs, the sensor was wiped clean as directed before. The muddy water was disposed from the bottle by pouring down the sink. The nozzle was cleared out by spraying until no further liquid exited. This ensured none of the solution from the previous test remained within the bottle. This process was then repeated four more times, but each time an extra scoop or approximately 1.5 g was added making the solution more concentrated with clay powder, hence creating more opaque droplets. The entire procedure is outlined in Figure 9.

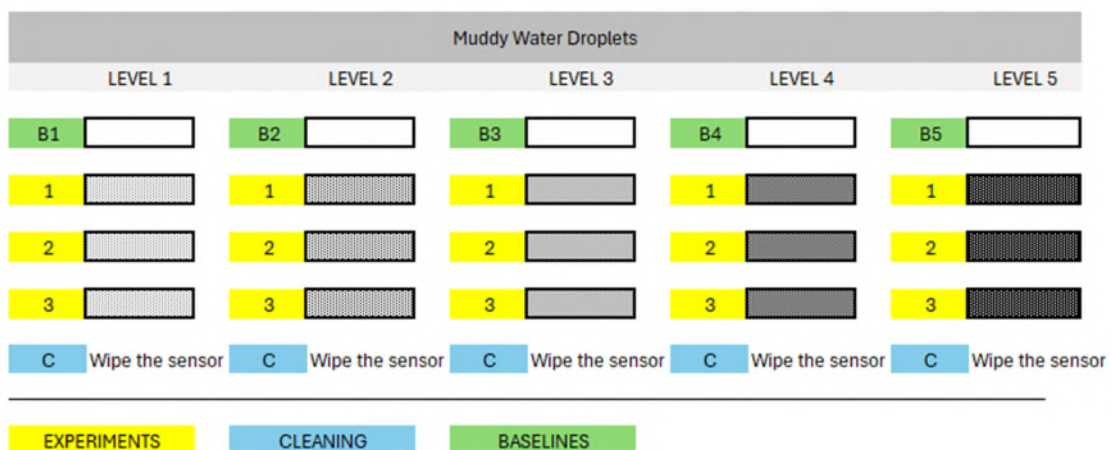


Figure 9: Experimental design for muddy water droplets study.

## 2.6. Quantifying the Percentage of LiDAR's Active Face Affected by the Noise Factors

The sprayer bottle shown in Figure 1 contains an adjustable nozzle mechanism capable of modifying the fineness of the water mist, thereby manipulating the size of water droplets created on LiDAR. However, the amount of droplets on the sensor's surface also depends on the duration of trigger actuation and the angle at which the spray is applied relative to the sensor plane. This can introduce potential inconsistencies in LiDAR's front face occlusion across the experiments. Consequently, evaluating the level of droplet occlusion based solely on the number of sprays becomes problematic, necessitating other quantitative approaches.

One way of achieving this is by utilising a DSLR camera to capture photos of the active face of the LiDAR after applying noise factors, as discussed in Section 2.3. These images can then be processed in MATLAB to identify the droplets on the sensor's surface using image recognition and processing techniques. Once the droplets have been identified, the proportion of the LiDAR's front face affected by the droplets can be quantified. The specific algorithms used to accomplish this are described in the following sections.

### ■ Imbinarise Image Processing Method

Imbinarise is a built-in MATLAB function that takes a greyscale image and sets all the pixels to either one or zero based on a user-defined threshold value for brightness. This works well in most scenarios where water droplets are present, as they usually appear in the image foreground and are usually denoted with higher pixel brightness due to internally reflecting the light source, which makes them brighter than other objects in the image. This can be seen in Figure 10. However, Imbinarise is vulnerable to noise from light sources captured in the image, such as the sun, which can be particularly problematic in outdoor images, as shown in Figure 11. This could potentially reduce the accuracy of identifying the percentage of the sensor screen obscured by water droplets.

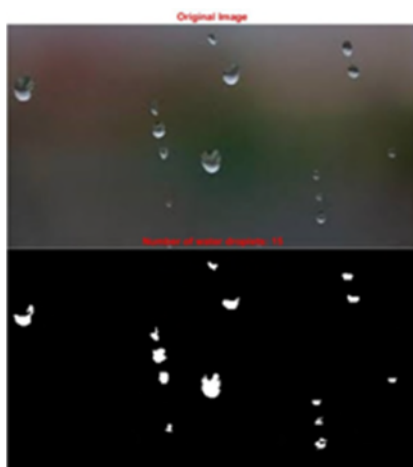


Figure 10: Imbinarise simpler example.



Figure 11: Imbinarise more challenging example.

- **Canny Edge Detection**

Canny Edge Detection is an image recognition algorithm that works by detecting the ridges in the image caused by a gradient magnitude in pixels around these edges. The algorithm then traces these ridges and sets all the pixels that are not on top of the ridge to zero and the pixels along the ridge to one. This allows for the detection of irregular shapes and the detection of smaller water droplets that might be overlooked by the Circle Hough Transform algorithm, as illustrated in Figure 12. This algorithm, however, detects all the edges in the image including objects in the background such as trees or signage which commonly occur along the roadside, as illustrated in Figure 13. This challenge could be addressed by combining Canny Edge Detection with other image recognition techniques to filter out unwanted objects, but this may inadvertently lead to some data loss.



Figure 12: Canny Edge Detection simpler example.



Figure 13: Canny Edge Detection more challenging example.

- **Combining Morphological Operations with Canny Edge Detection and Imbinarise**

Morphological operations encompass a wide range of image processing techniques that process images based on shapes. In a morphological operation, each pixel in the image is adjusted based on the value of other pixels in its neighbourhood. By choosing the size and shape of the neighbourhood, it is possible to construct a morphological operation that is sensitive to specific shapes within the input image.

Canny Edge Detection provides the outlines of edges of all the objects within a frame. However, water droplets are circular in nature and using the morphological operations it is possible to highlight only these “disks” rather than the lines. Furthermore, using the function “imclose” any circular features that may have gaps or are not fully closed as seen in Figure 14, will be completed allowing the morphological operation “imfill” to fill these holes as white

dots, which is better illustrated in Figure 15. This can be particularly useful in the scenario where a camera is positioned to take an image of the LiDAR active face to quantify the percentage of LiDAR screen area affected by water droplets.

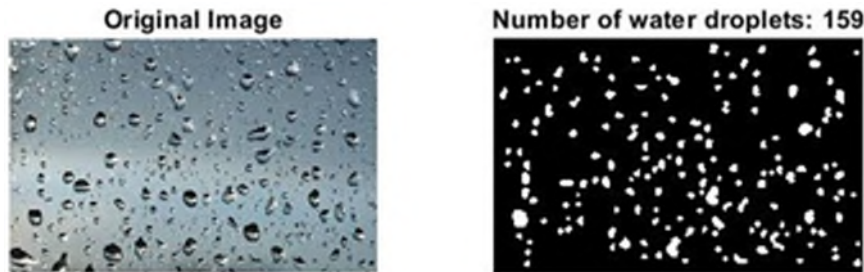


Figure 14: Canny Edge Detection with Morphological Operations.



Figure 15: Canny Edge Detection with Morphological Operations.

#### ■ Processing the Images from the Laboratory Experiments

Before using MATLAB to process the images, the images had to be cropped to only contain the front face of the sensor. The DSLR camera outputted the images files in two file formats, out of which only the JPG was used. To improve algorithm performance, these cropped images had their brightness and exposure increased to 100% while decreasing the contrast to -100% using a photo editor application. The two different methods were used in tandem to achieve optimal results when processing the images captured in the laboratory.

It was observed that Canny Edge Detection produced better results than the Imbinarise when attempting to identify the water droplets. This was because some water droplets were transparent, not reflecting the flash of the camera or room lights, which lead to significantly lower percentages outputted.

However, as the muddy droplets were somewhat opaque, the Imbinarise produced satisfactory results and performed better than the Canny Edge Detection. With larger droplets, though their edges were detected, the Canny Edge Detection struggled to close these large areas. To combat this, the parameter to set the size of the disk to be filled was increased. However, this caused multiple droplets to be combined as one chain and outputted substantial portions of the image to have supposedly been affected.



Our code iterates through a folder of the images and applies the chosen algorithm, the result of which is then outputted as a figure. The output figure contains two images: the original image and the binary image highlighting the droplets, along with a percentage indicating how much of the image is covered in droplets. The image name and the percentage output are then saved to a CSV file, and the processed image is saved to the same folder. Examples of the outputs can be seen in Figure 16 and Figure 17.

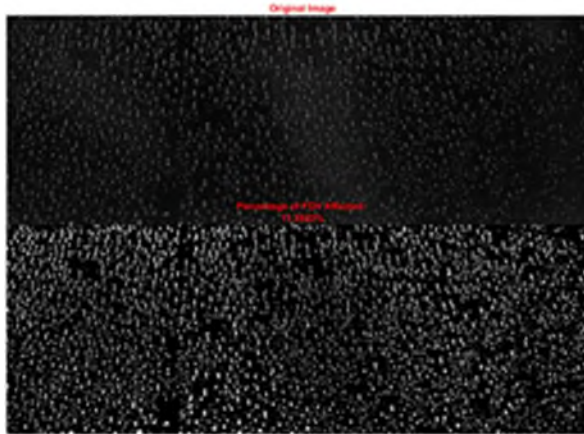


Figure 16: Clear water droplet detection output using Canny Edge Detection.

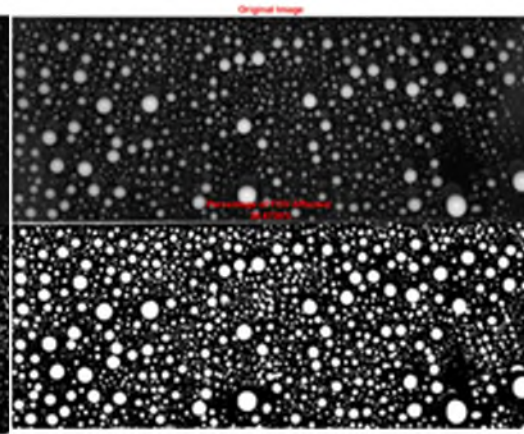


Figure 17: Muddy water droplet detection output using Imbinarise.

#### ■ Quantifying the impact on LiDAR point cloud

To quantify the potential impact of noise factors on point clouds, first we computed the number of points (point count) in a single frame or the baseline point cloud, which was recorded with a clean sensor. For an occluded sensor, 11 frames were selected from the point cloud and its number of points counted, then expressed as a percentage of the point count of the baseline frame. Therefore, a relative point count was computed for each frame. Finally, the average and standard deviation of the relative point count was calculated across the 11 frames to characterise the point cloud recorded under a droplet occlusion. The hypothesis was that droplet occlusions might block some of the LiDAR beams leaving or entering the sensor, thereby reducing the overall point count.

Another crucial metric was the intensity of points in the LiDAR point cloud. This was, however, computed not on the entire point cloud but only on the points falling on a calibrated reflectance board. Figure 18 shows the visualisation of the entire point cloud capturing the experimental area, as well as the cropping and extraction of the points belonging solely to the calibrated reflectance board. Average intensity and standard deviation of intensity of those points were computed to investigate the impact of droplet occlusion on LiDAR intensity. The hypothesis was that droplet occlusions would reduce the intensity by absorbing some of the energy of the LiDAR beams.

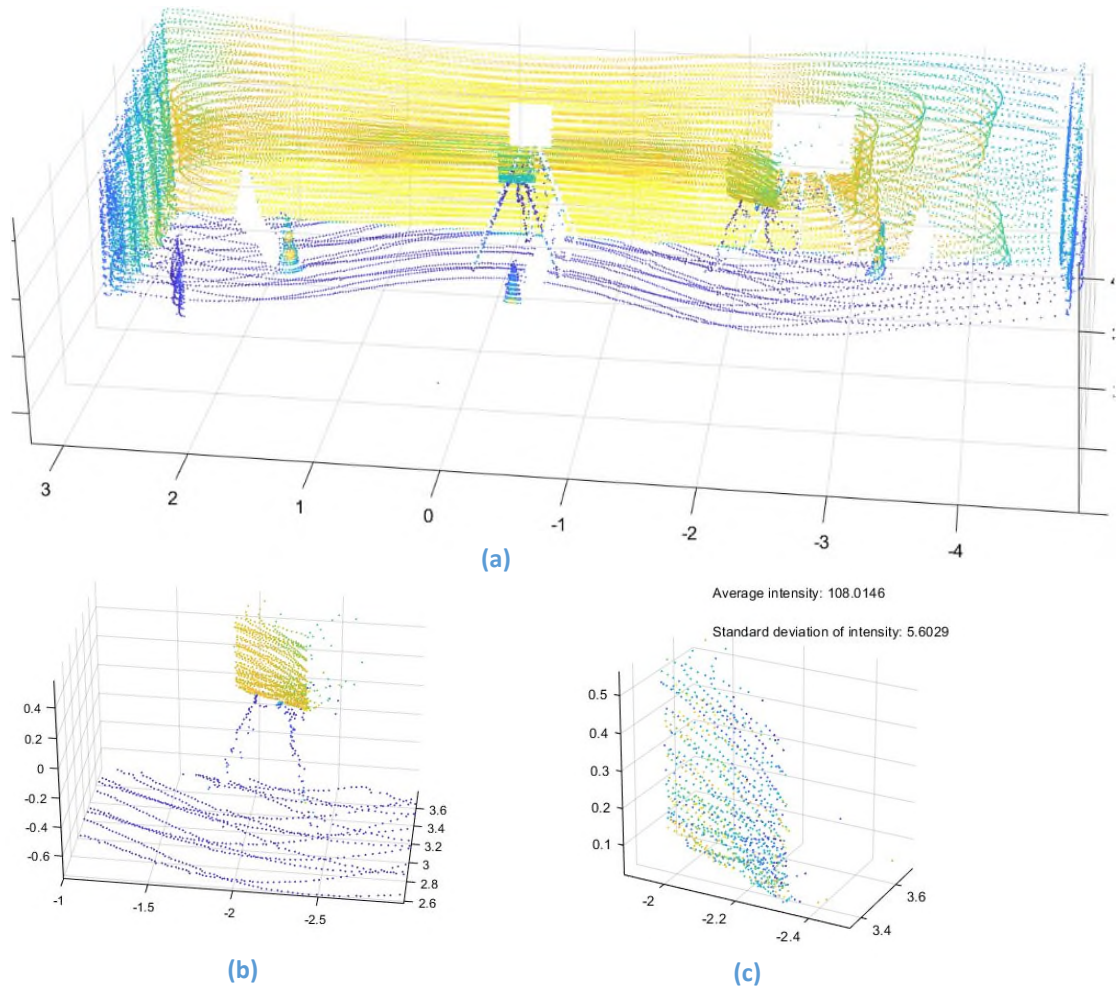


Figure 18: : (a) LiDAR point cloud showing the entire experimental area with targets; (b) cropped area including one reflectance board; (c) isolated points of the calibrated reflectance board and intensity metrics.

## 2.7. Results

### ■ Clear Water Droplets

Figure 19, Figure 20, and Figure 21 show the relationship between the clear water droplet coverage (the percentage of LiDAR front screen area covered by clear water droplets) and the relative point count (the number of points in the occluded point cloud compared to the number of points in the baseline point cloud recorded with a clean screen), for LiDAR A, LiDAR B, and LiDAR C, respectively. Each sphere represents one point cloud recording with its size proportional to the standard deviation of the relative point count. The linear regression trend line was estimated assuming the intercept of 100% because the baseline point cloud was recorded with 0% droplet coverage and its relative point count is 100%.

For LiDAR A and LiDAR C a weak negative relationship was observed between the independent and dependent variables, suggesting that even clear water droplets might have some ability to block LiDAR beams and reduce the number of points in the point cloud. For LiDAR B, the

relative point count seemed almost unaffected by the amount of water droplet coverage, suggesting that the longer wavelength LiDAR (1550 nm) might be more robust compared to the wavelength of 905 nm.

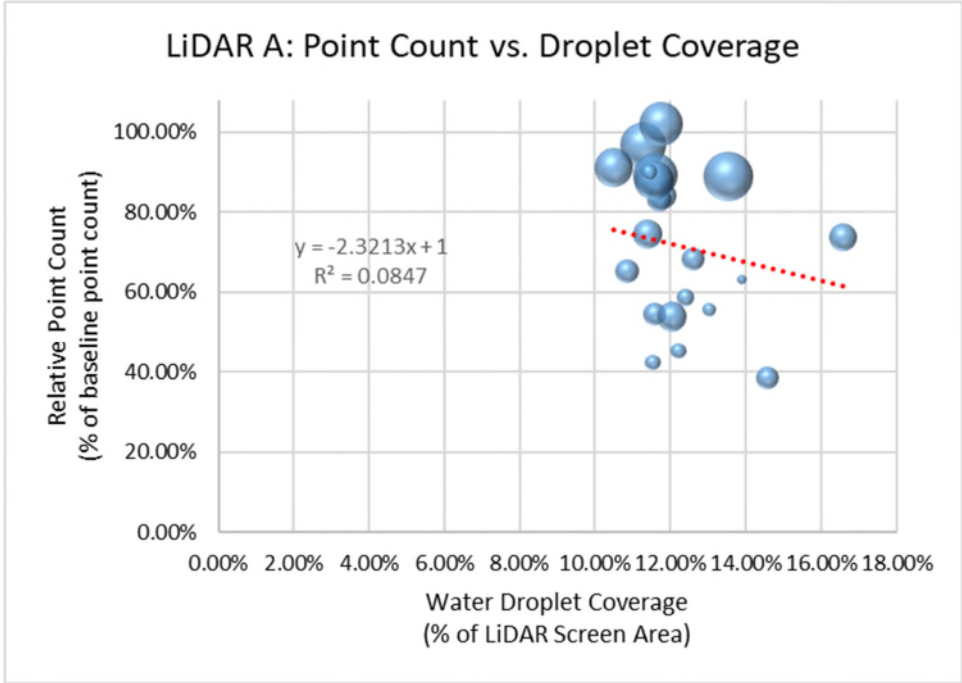


Figure 19: Relationship between the clear water droplet coverage and the relative point count for LiDAR A.

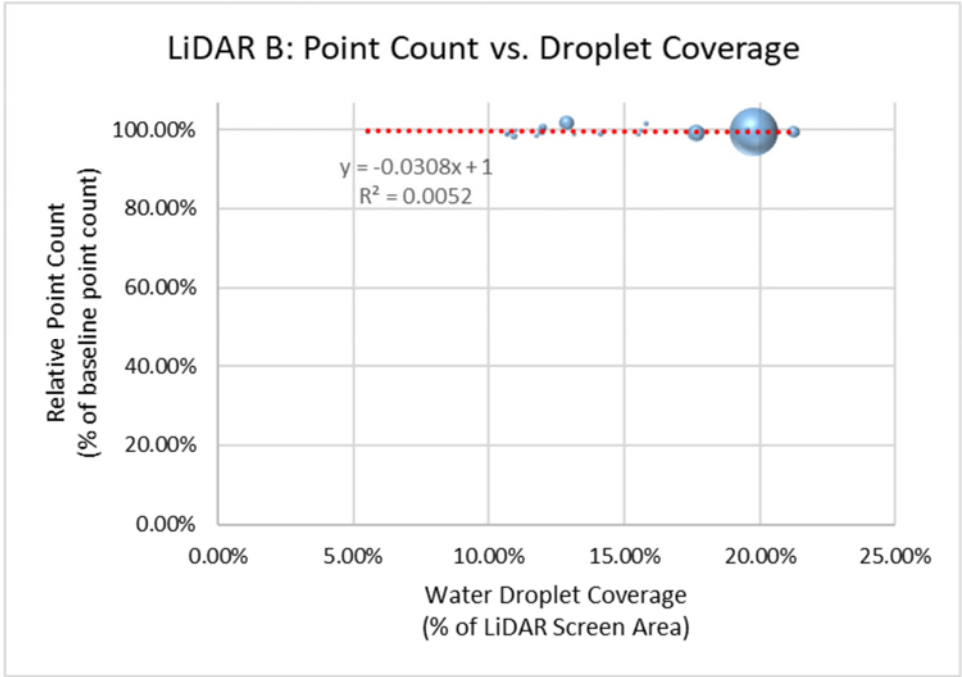


Figure 20: Relationship between the clear water droplet coverage and the relative point count for LiDAR B.

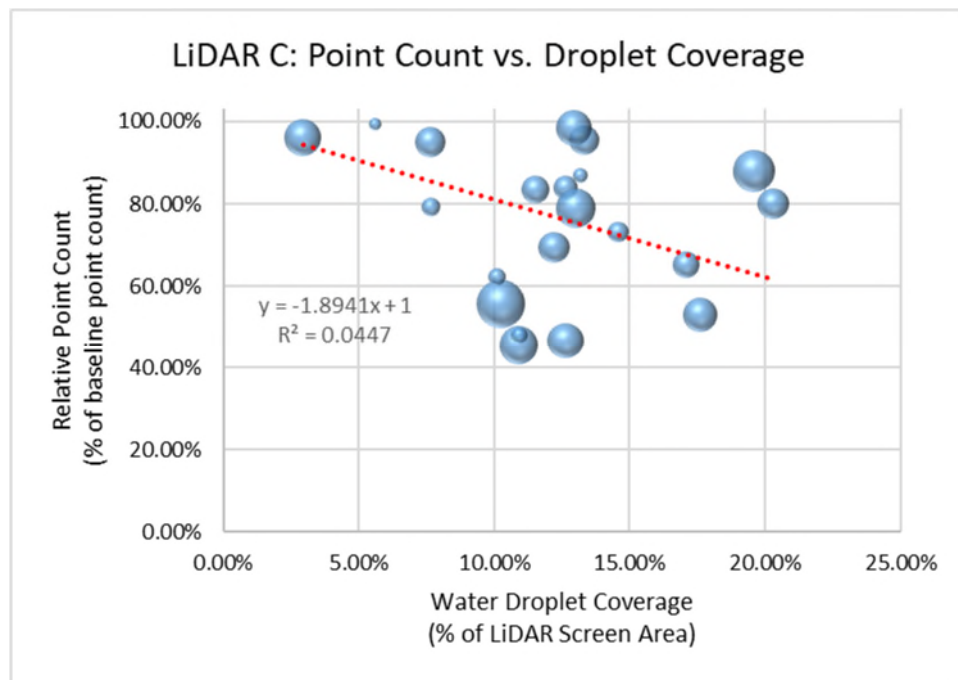


Figure 21: Relationship between the clear water droplet coverage and the relative point count for LiDAR C.

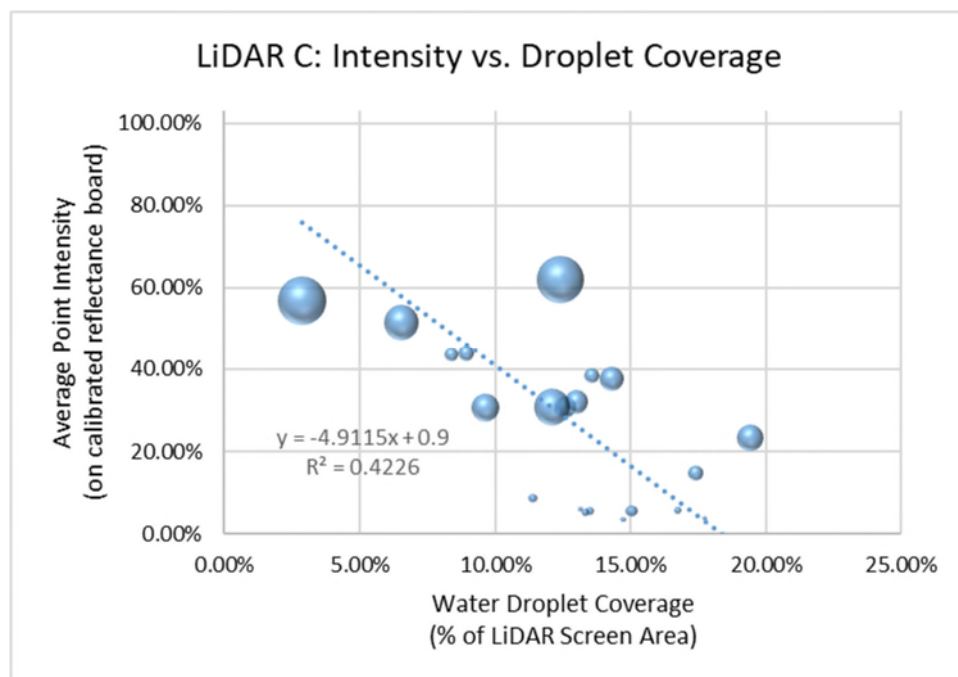


Figure 22: Relationship between the clear water droplet coverage and average point intensity on the calibrated reflectance board.

For LiDAR C a strong negative relationship was observed between the coverage percentage and the average intensity of points on the calibrated reflectance board (see Figure 22). This suggest that the impact of clear water droplet occlusion might be manifesting more as a decreased intensity rather than a marked decrease in the point count, which would occur if the beams were strongly absorbed or fully blocked.

### ■ Muddy Water Droplets

Figure 23, and Figure 24, and Figure 25 depict the relationship between muddy water droplet coverage (the percentage of LiDAR front face covered by muddy water droplets) and relative point count (the number of points in the occluded point cloud compared to the number of points in the baseline point cloud recorded with a clean screen) for LiDAR A, LiDAR B, and LiDAR C, respectively. The negative relationship between the droplet coverage and the number of points speaks to the ability of muddy water droplets to block LiDAR beams and reduce the number of points in the point cloud. For LiDAR B, however, the  $R^2$  value is almost zero, which could be a consequence of low variability in droplet coverage across the experiments.

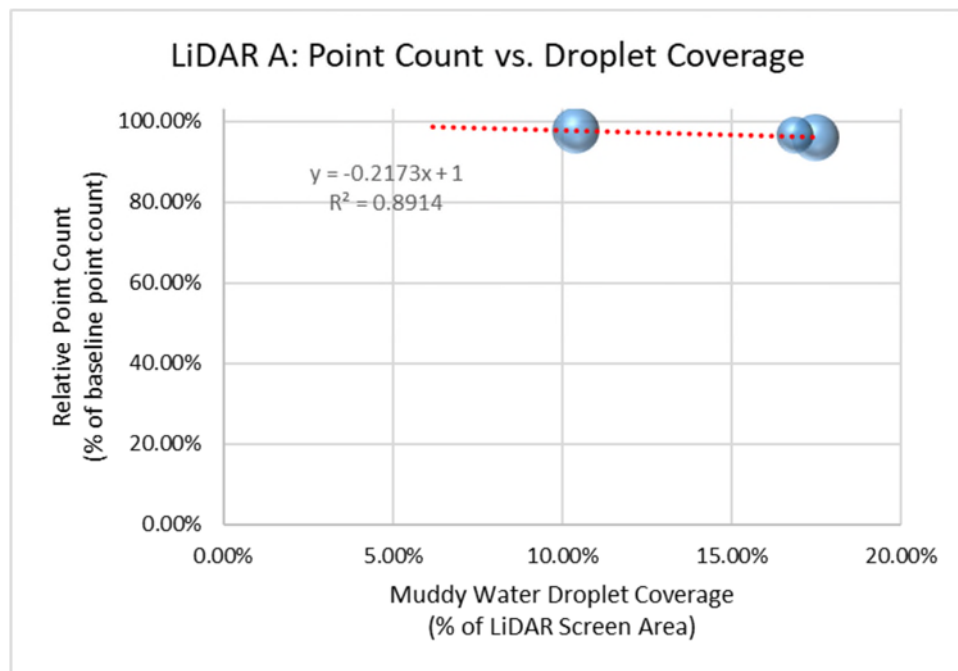


Figure 23: Relationship between the muddy water droplet coverage and the relative point count for LiDAR A.

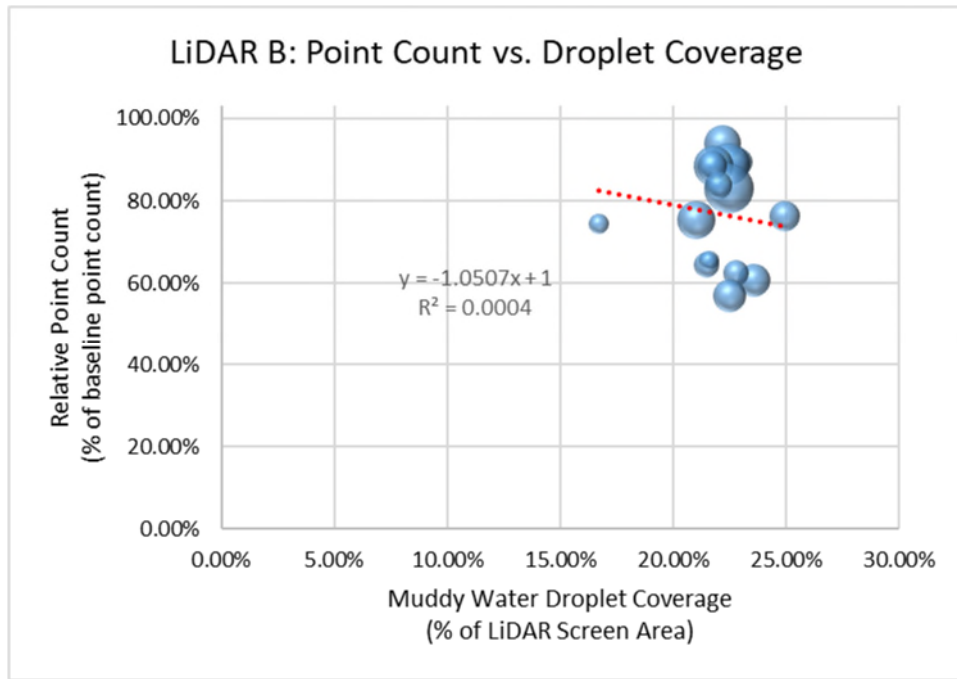


Figure 24: Relationship between the muddy water droplet coverage and the relative point count for LiDAR B.

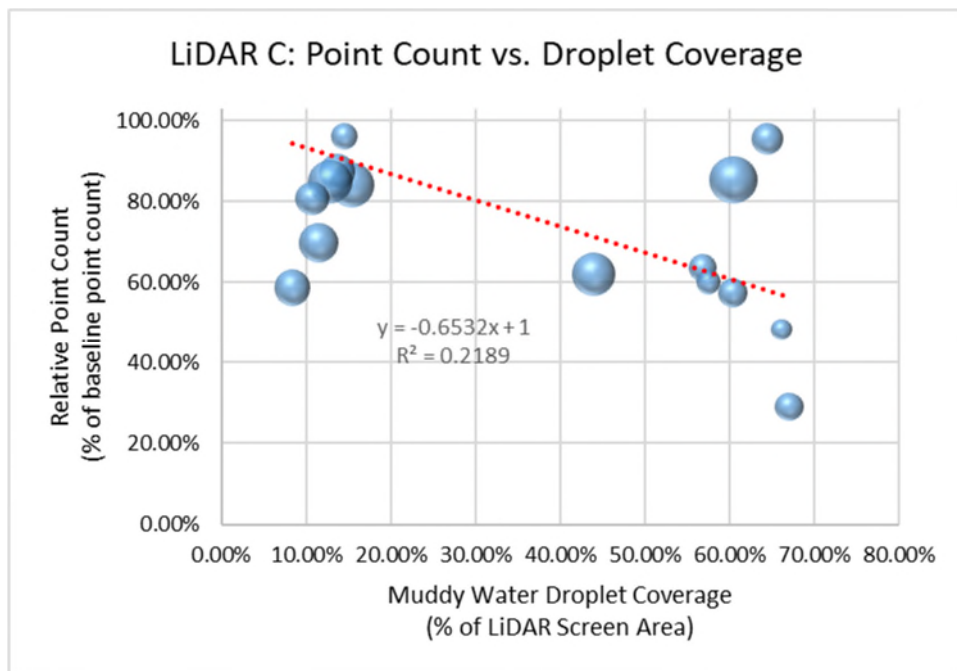
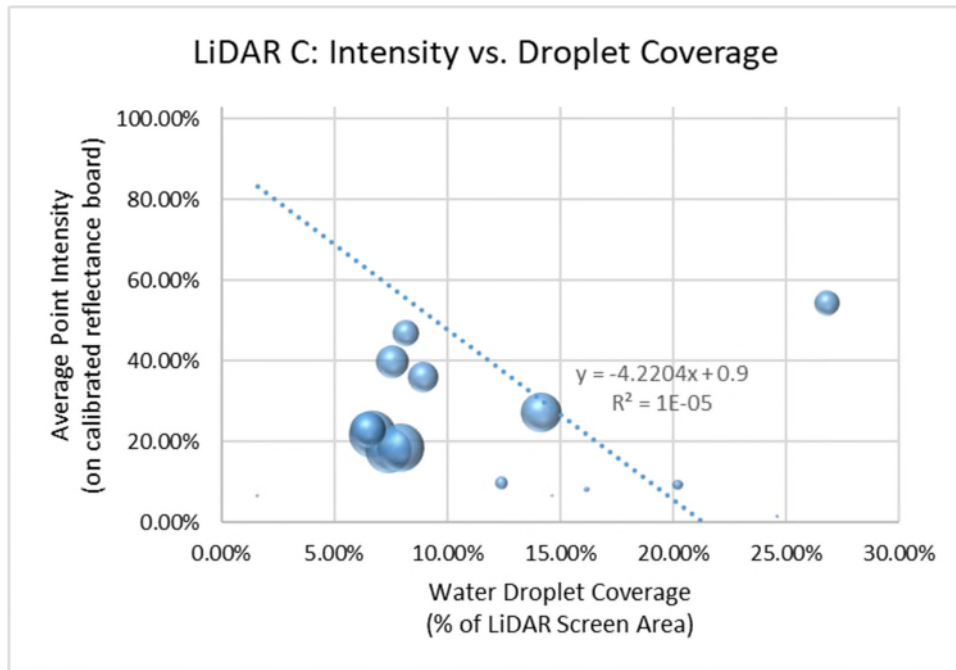


Figure 25: Relationship between the muddy water droplet coverage and the relative point count for LiDAR C.





**Figure 26: Relationship between the muddy water droplet coverage and average point intensity on the calibrated reflectance board.**

For LiDAR C additionally, no relationship was observed between the coverage percentage and the average intensity of points on the calibrated reflectance board (see Figure 22), despite forcing the 90% intercept, as can be seen in the  $R^2$  value of almost zero. This suggests that muddy water droplet occlusion might manifest more via blocking the beams (reducing the point count) rather than reducing the point intensity.

Lastly, we examined the impacts of the varying mud concentration (the amount of clay powder in the muddy water). Figure 27 shows the relationship between the mud concentration level and the percentage of the surface area of the LiDAR front screen covered by the muddy water droplets, for three LiDARs combined. As can be seen from the Box and Whisker plot, higher mud concentration leads to higher coverage of the LiDAR front screen. This could be the result of multiple factors. Firstly, the Imbinarise algorithm might be better at detecting muddier water droplets due to their higher opaqueness. Secondly, muddy water droplets with higher mud concentration might have better ability to grip onto the LiDAR screen due to increased viscosity. Higher mud concentrations also lead to lower relative point count for three LiDARs combined (see Figure 28), demonstrating the ability of clay particles to interact with LiDAR beams.

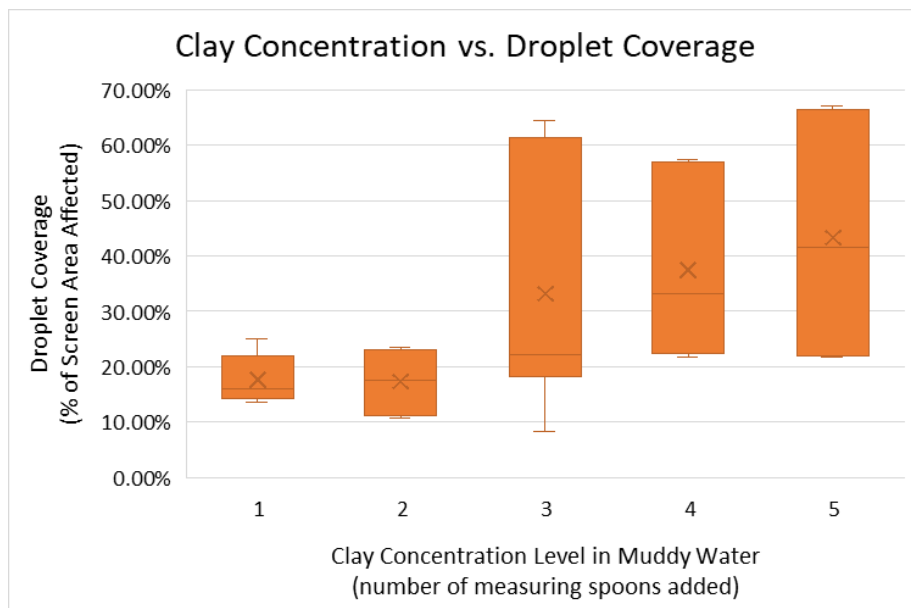


Figure 27: Relationship between clay concentration level and muddy water droplet coverage.

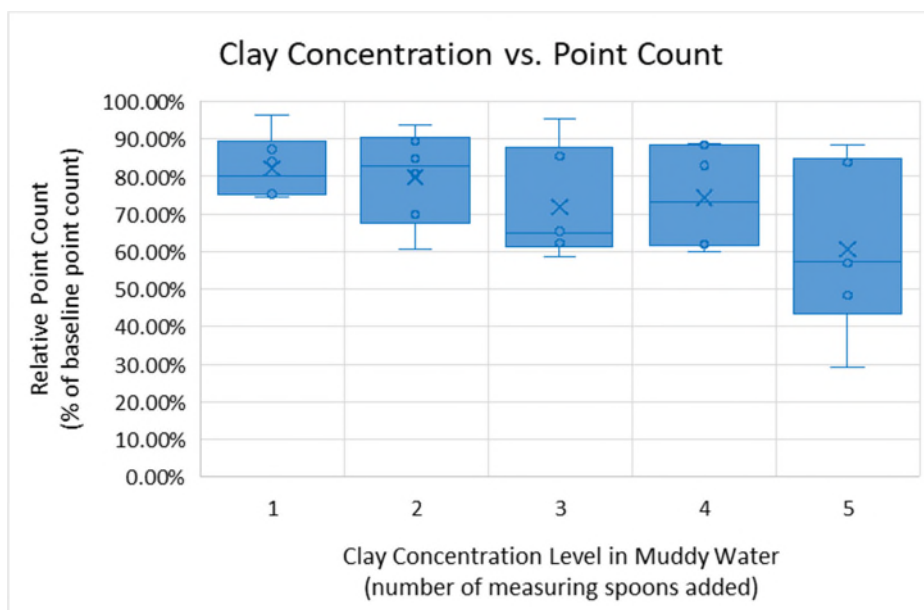


Figure 28: Relationship between the mud concentration level and relative point count.



### 3. Conclusions

This report introduces a novel methodology for studying LiDAR noise factors, based on experimental data collected in the WMG Perception Sensors Testing Laboratory. The study focused on the effects of direct LiDAR occlusion caused by clear water droplets and muddy water droplets.

The proposed method presents a replicable procedure using simple tools and a safe chemical – a type of clay powder – that poses no health hazards (e.g., it contains no silica dust) and has no workplace exposure limits (unlike the kaolin clay). However, PPE (glasses, gloves, mask) were still used in accordance with the chemical's Safety Data Sheet.

Several limitations of this method for creating occlusions were identified:

- Although clay powder is a key component of the real mud, it may not be fully representative of the complexity of real mud which is comprised of many substances of varying particle sizes.
- The clay powder used in experiments is somewhat hydrophobic, leading to clumping and difficulty in mixing it into a homogeneous liquid.
- The sprayer bottle used did not guarantee consistent amounts dispersed with each spray. It also occasionally struggled with clumps in the muddy water.
- Clear water droplets tended to agglomerate and leak down the sensor, creating streaky marks. In contrast, muddy water was found to adhere better to the LiDAR surface, likely due to increased viscosity.
- Spraying muddy water proved somewhat messy, as it could enter the crevices of the LiDAR device, complicating the cleaning process. Covering parts of the LiDAR with paper towels alleviated some of this problem, but not entirely.
- Despite the small size of clay particles, wiping them off the LiDAR active surface could result in microscopic scratches, potentially damaging the device and compromising data quality.

The method of using images of the LiDAR front screen to quantify droplet coverage appears appropriate, although the following limitations were observed:

- As LiDAR front faces are made of a transparent material (glass), they can exhibit mirroring effects. This can result not only with the camera and flash showing in the photo of the LiDAR but also as many droplet occlusions being shown double.
- The photo of the LiDAR front face does not capture the curvature of the front face, so the method may not work for curved faces as well as for flat LiDAR faces.
- After taking the picture of the LiDAR front face, the tripod-mounted camera must be removed for each data collection. This means it is difficult to ensure that the camera is always in the exact same position and orientation.
- The algorithms used for computing the LiDAR coverage with clear or muddy droplets are not flawless, which means they can potentially underestimate or overestimate the real coverage. This can be observed in some of the examples shown in the Appendix.

- Furthermore, the active area of the LiDAR front face – through which beams leave/enter the sensor – is smaller than the full screen area. In our coverage computation, we considered the entire screen of the LiDAR. However, we also recomputed the coverage by assuming a perimeter of 10% width/height as the inactive area, but this did not significantly alter the results or conclusions. This suggests the droplets were relatively homogeneously distributed across the active face in our experiments, which may not always be the case in real-life conditions.

The key takeaways from this research are the following:

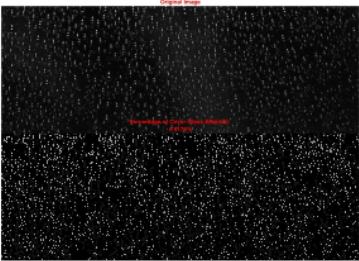
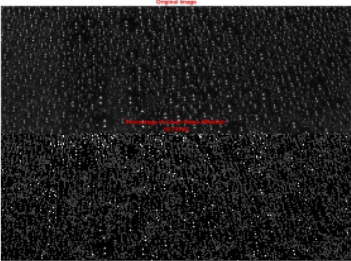
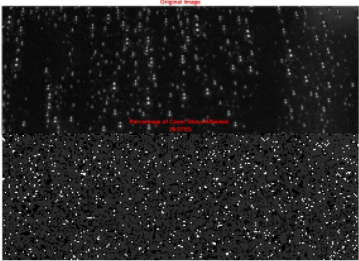
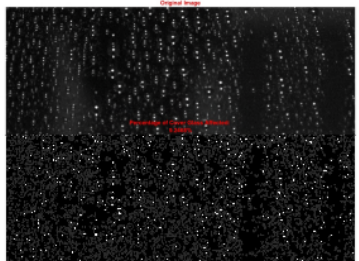
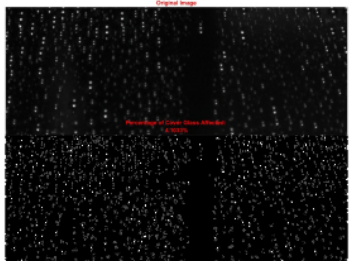

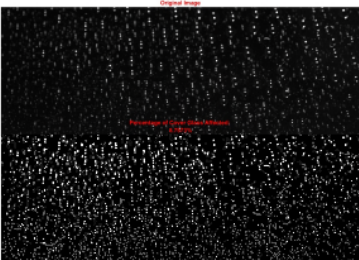
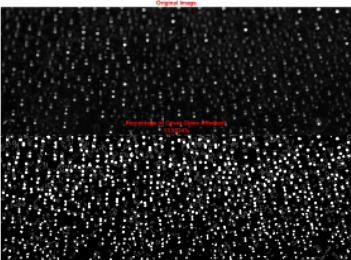
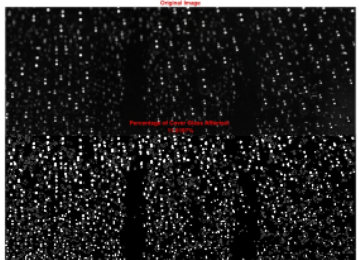

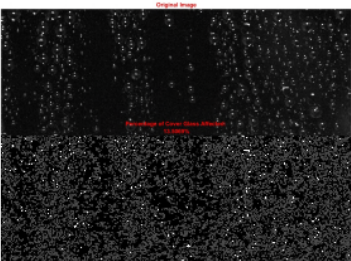
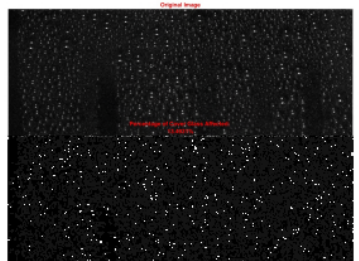
- LiDAR occlusions have a marked potential to impact data quality, which could further compromise its performance as automotive perception sensors.
- Muddy water droplets, and mud splashes in particular, are problematic as they can block infrared beams, creating missing information in the point cloud. Unlike mud splashes which block 100% of the beams, muddy water is typically semi-transparent depending on the concentration of mud.
- Clear water droplets, however, also present potential problems, as evidenced by their impact on the point cloud, affecting both the number of points and their intensity.
- The 1550 nm wavelength LiDAR appears to be (potentially) more robust against clear water droplet occlusion compared to the 905 nm wavelength LiDAR, although further research is needed to confirm this.
- For real-world applications of automotive LiDAR sensors as part of automated driving systems (ADS) or advanced driver-assistance systems (ADAS), regular cleaning of sensor surfaces from soiling and occlusion is essential to prevent data degradation and ensure reliable and safe deployment.

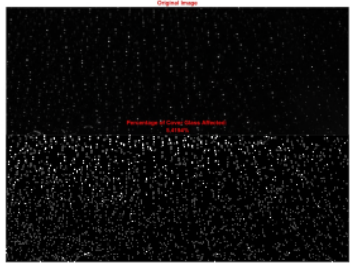
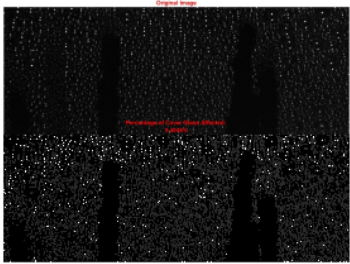
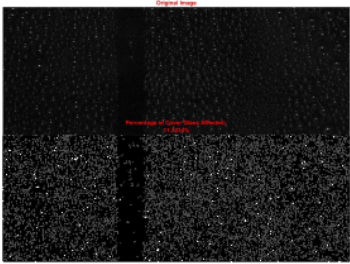
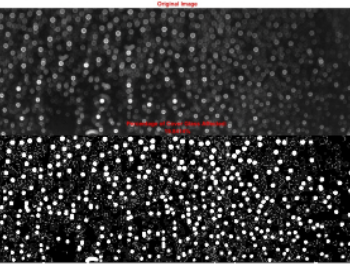
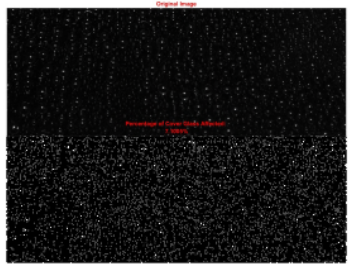
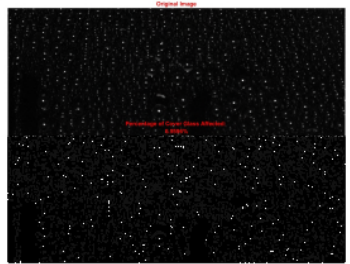
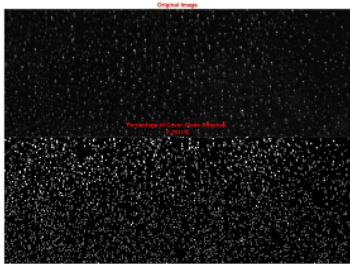
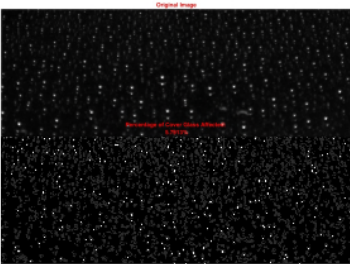
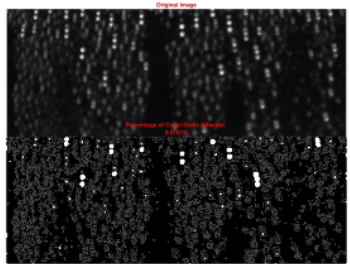
# Appendix I – Datasets

This Appendix includes the images of occluded LiDAR front faces for all the experiments.

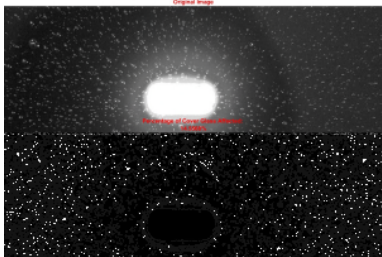
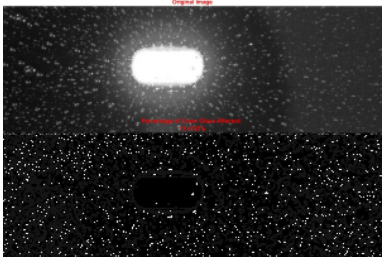
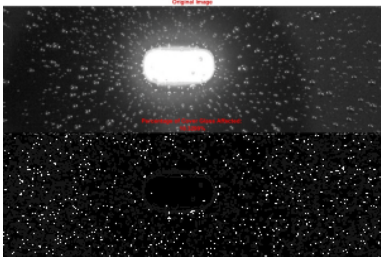
## 3.1. Water Droplets

### ■ LIDAR A

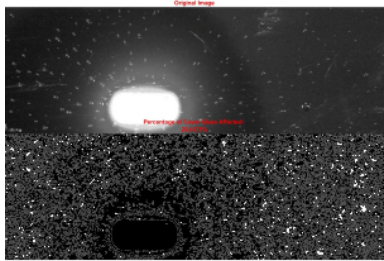
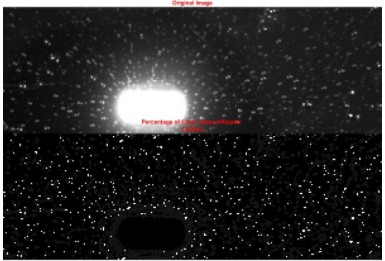
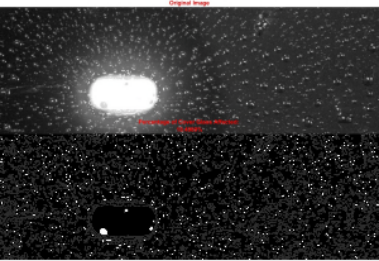
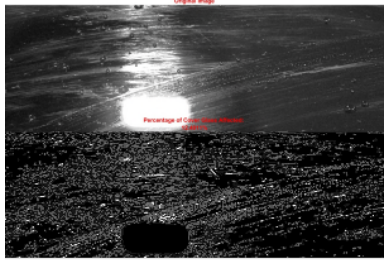
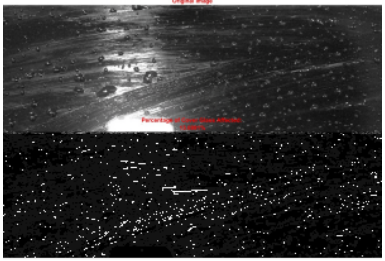
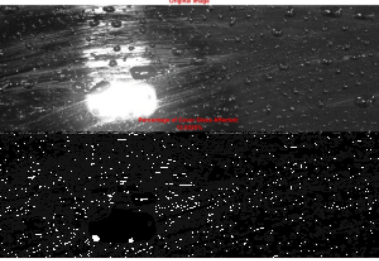

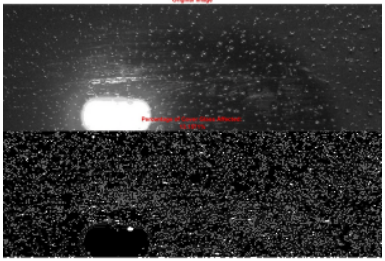
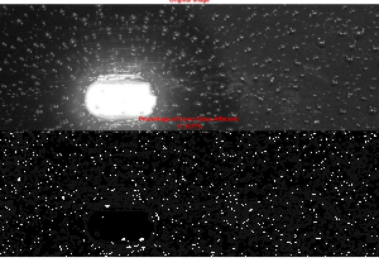

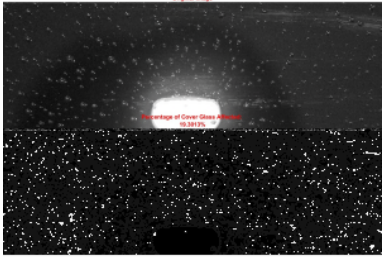
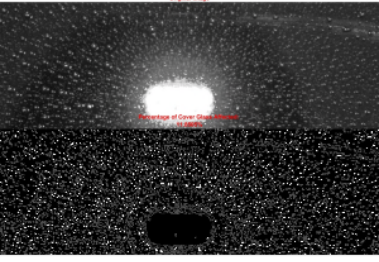
| Test Set A  |   |   |
|---|---|---|
| Test 1  | Test 2  | Test 3  |
|    |    |    |
| 8.02%   | 10.75%  | 20.08%  |
| Test Set B  |   |   |
| Test 1  | Test 2  | Test 3  |
|   |   |   |
| 9.25%   | 4.1%  | 8.81%   |
| Test Set C  |   |   |
| Test 1  | Test 2  | Test 3  |
|  |  |  |
| 8.76%   | 13.97%  | 11.62%  |
| Test Set D  |   |   |
| Test 1  | Test 2  | Test 3  |
|  |  |  |
| 17.29%  | 13.51%  | 13.49%  |

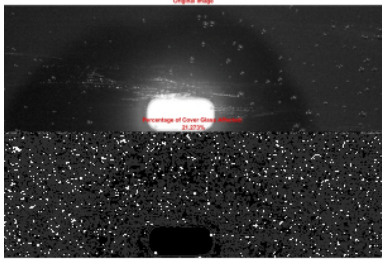
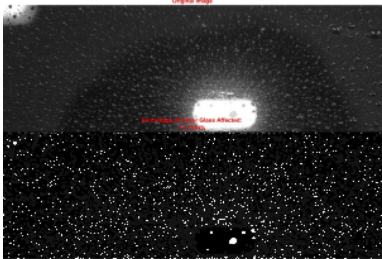
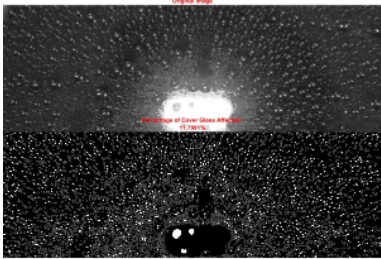

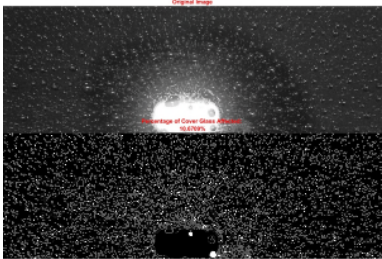
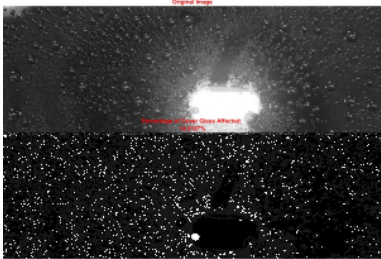
| Test Set E  |   |   |
|---|---|---|
| Test 1  | Test 2  | Test 3  |
|    |    |    |
| 5.42%   | 9.4%  | 11.32%  |
| Test Set F  |   |   |
| Test 1  | Test 2  | Test 3  |
|    |    |    |
| 19.84%  | 7.1%  | 6.96%   |
| Test Set G  |   |   |
| Test 1  | Test 2  | Test 3  |
|  |  |  |
| 7.75%   | 5.79%   | 9.08%   |

## - LiDAR B

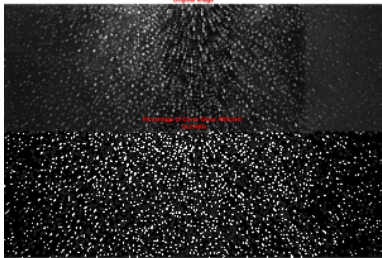
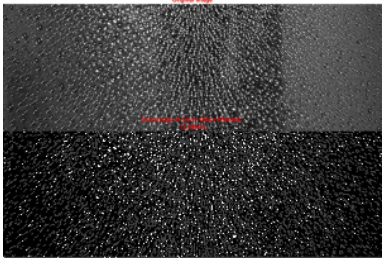
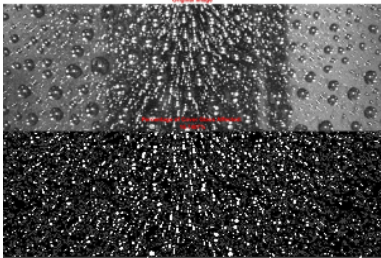
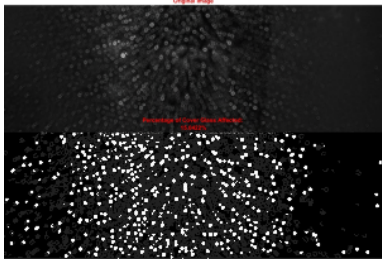
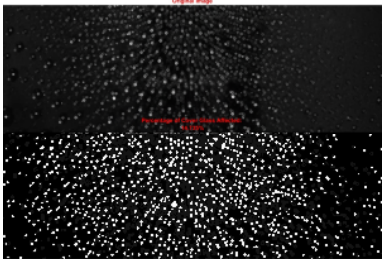
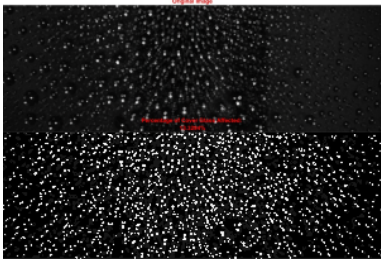
| Test Set A  |   |   |
|---|---|---|
| Test 1  | Test 2  | Test 3  |
|  |  |  |
| 14.56%  | 11.47%  | 10.33%  |



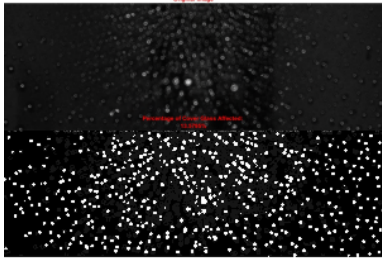
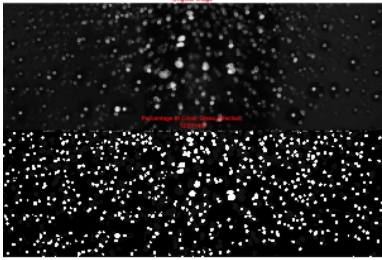
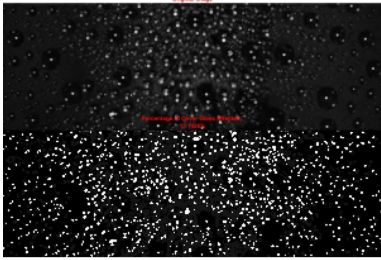
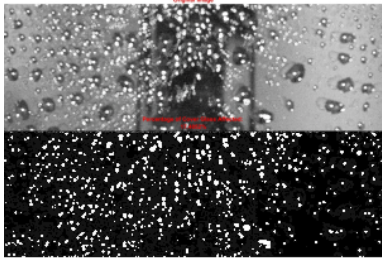
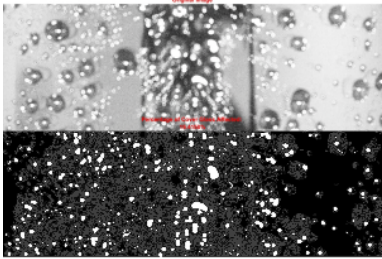
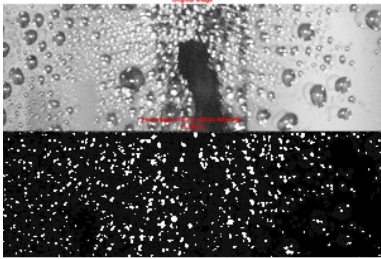
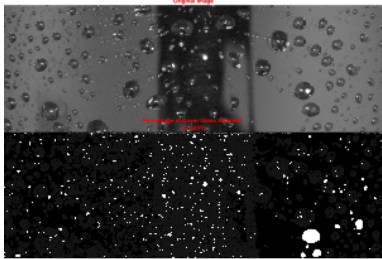
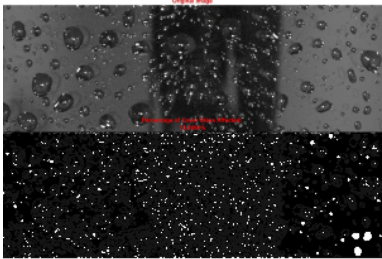
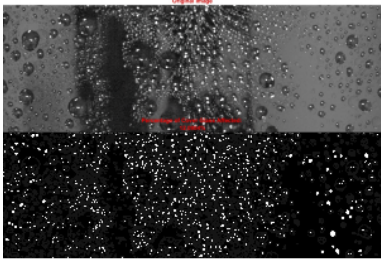
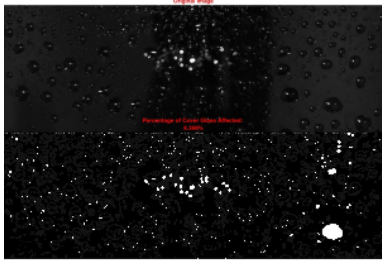
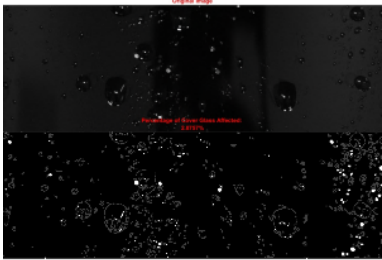
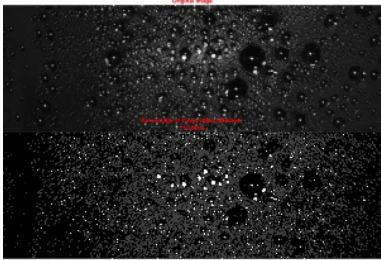
| Test Set B  |   |   |
|---|---|---|
| Test 1  | Test 2  | Test 3  |
|    |    |    |
| 20.64%  | 5.84%   | 10.49%  |
| Test Set C  |   |   |
| Test 1  | Test 2  | Test 3  |
|    |    |    |
| 12.4%   | 13.7%   | 12.93%  |
| Test Set D  |   |   |
| Test 1  | Test 2  | Test 3  |
|  |  |  |
| 16.6%   | 13.16%  | 11.32%  |
| Test Set E  |   |   |
| Test 1  | Test 2  | Test 3  |
|  |  |  |
| 19.48%  | 19.3%   | 11.85%  |
| Test Set F  |   |   |
| Test 1  | Test 2  | Test 3  |

|   |   |   |
|---|---|---|
|  |  |  |
| 21.27%  | 11.75%  | 11.8%   |
| <b>Test Set G</b>   |   |   |
| Test 1  | Test 2  | Test 3  |
|  |  |  |
| 10.95%  | 10.67%  | 14.21%  |

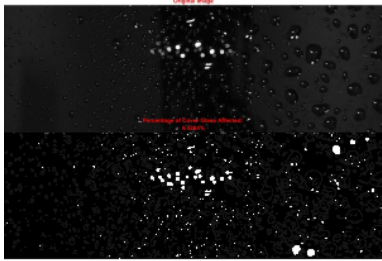
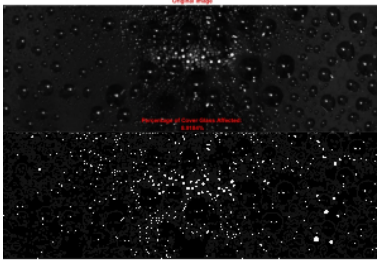
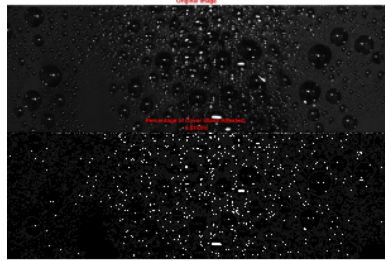
## ■ LiDAR C

|   |   |   |
|---|---|---|
| <b>Test Set A</b>   |   |   |
| Test 1  | Test 2  | Test 3  |
|  |  |  |
| 14.31%  | 13.49%  | 16.74%  |
| <b>Test Set B</b>   |   |   |
| Test 1  | Test 2  | Test 3  |
|  |  |  |
| 15.04%  | 14.74%  | 13.33%  |
| <b>Test Set C</b>   |   |   |



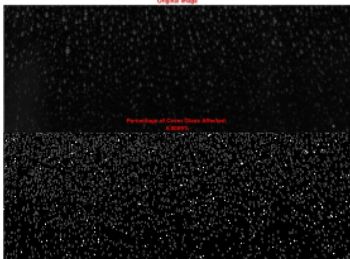

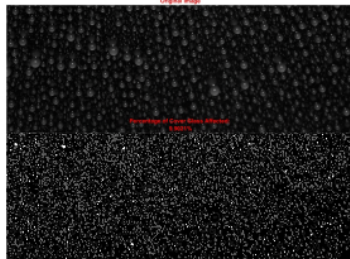
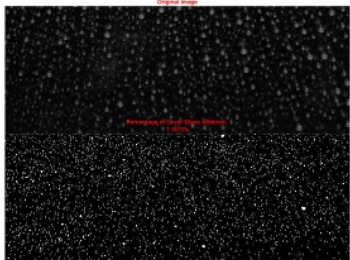
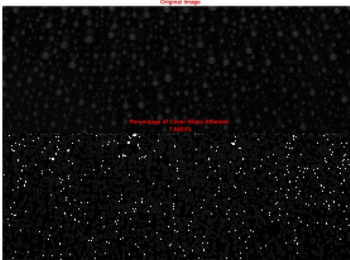



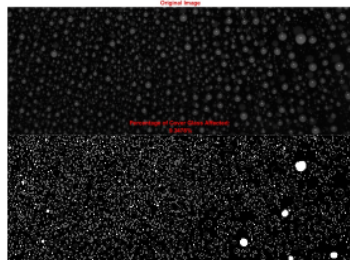

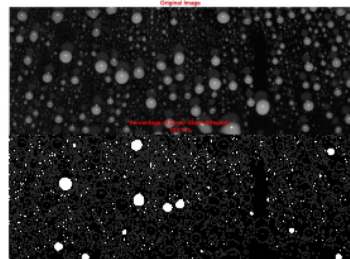

| Test 1  | Test 2  | Test 3  |
|---|---|---|
|    |    |    |
| 13.58%  | 12.61%  | 13.14%  |
| Test Set D  |   |   |
| Test 1  | Test 2  | Test 3  |
|    |    |    |
| 17.41%  | 19.42%  | 17.75%  |
| Test Set E  |   |   |
| Test 1  | Test 2  | Test 3  |
|  |  |  |
| 12.42%  | 13%   | 12.1%   |
| Test Set F  |   |   |
| Test 1  | Test 2  | Test 3  |
|  |  |  |
| 8.37%   | 2.88%   | 11.39%  |
| Test Set G  |   |   |
| Test 1  | Test 2  | Test 3  |

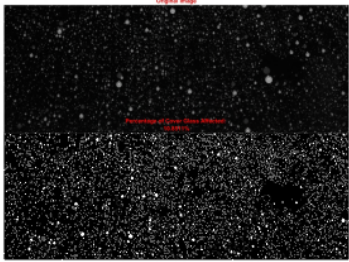
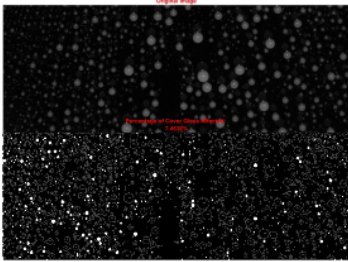
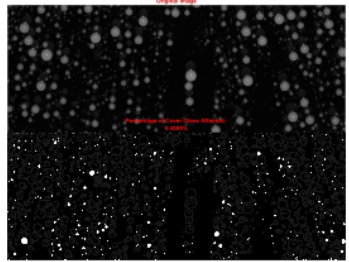
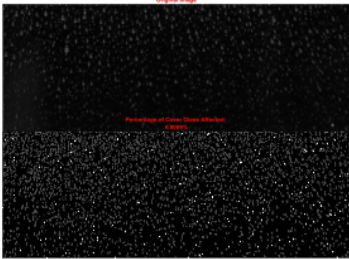
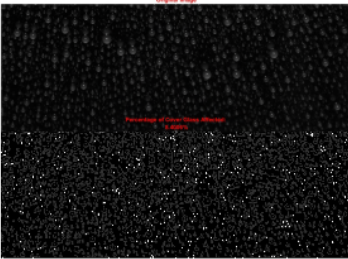
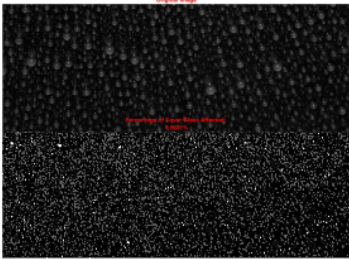
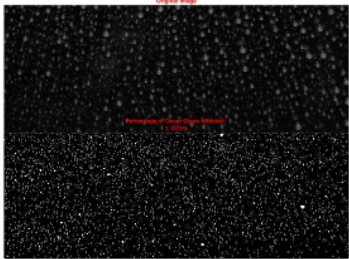
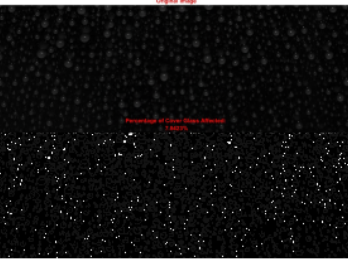
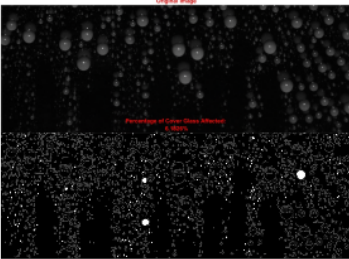
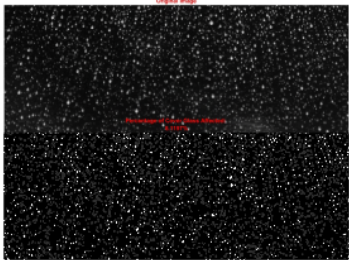
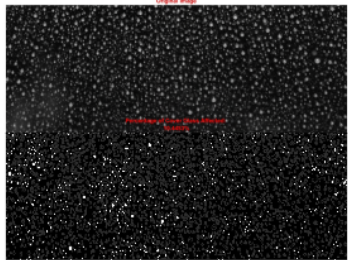
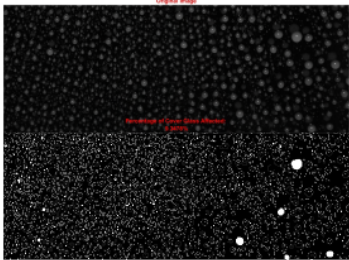


|  |  |  |
|--|--|--|
|  <p>Original Image</p> <p>Percentage of Dark Noise Removed: 6.53%</p> |  <p>Original Image</p> <p>Percentage of Dark Noise Removed: 8.92%</p> |  <p>Original Image</p> <p>Percentage of Dark Noise Removed: 9.62%</p> |
| 6.53%  | 8.92%  | 9.62%  |

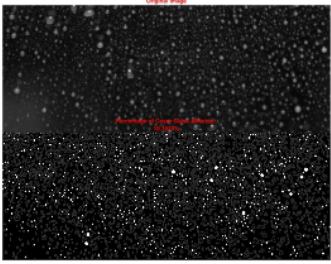
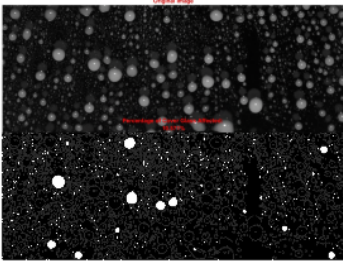

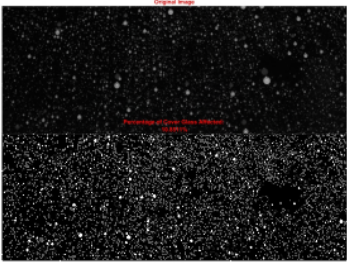
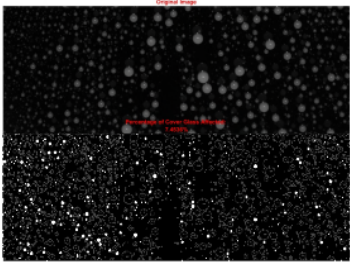
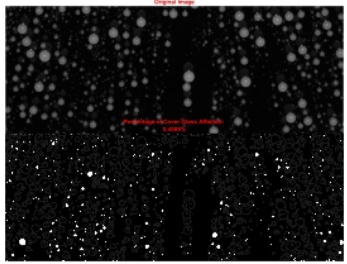
## 3.2. Muddy Water Droplets

### ■ LIDAR A

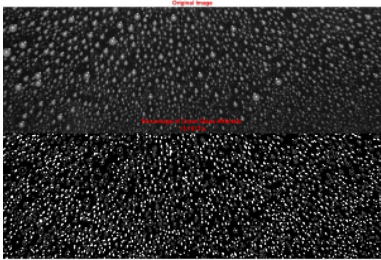
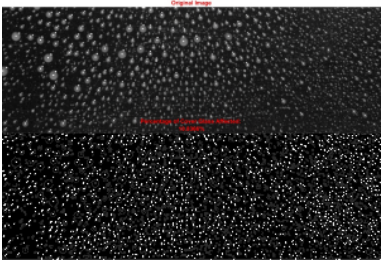
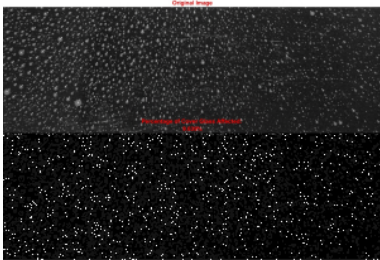
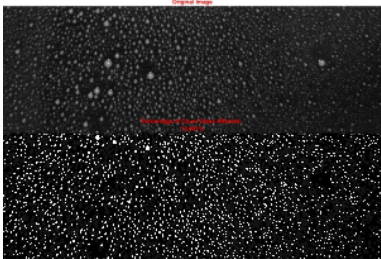
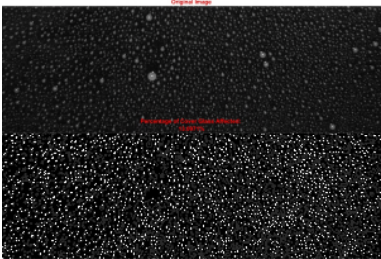

| Test Set A  |   |   |
|---|---|---|
| Test 1  | Test 2  | Test 3  |
|    |    |    |
| 6.8%  | 8.4%  | 9.9%  |
| Test Set B  |   |   |
| Test 1  | Test 2  | Test 3  |
|   |   |   |
| 7.2%  | 7.84%   | 6.18%   |
| Test Set C  |   |   |
| Test 1  | Test 2  | Test 3  |
|  |  |  |
| 8.12%   | 10.45%  | 9.35%   |
| Test Set D  |   |   |
| Test 1  | Test 2  | Test 3  |
|  |  |  |
| 10.31%  | 10.57%  | 7.75%   |
| Test Set E  |   |   |

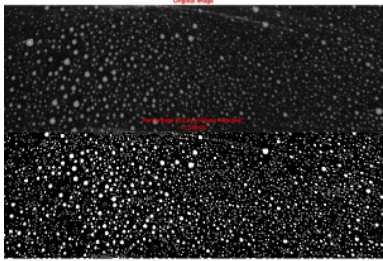
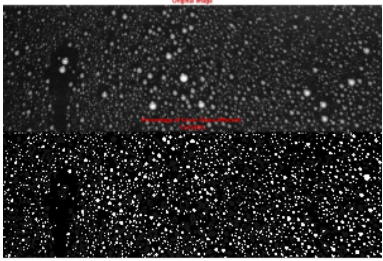
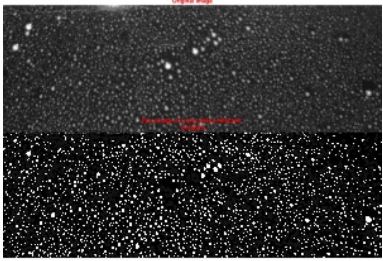
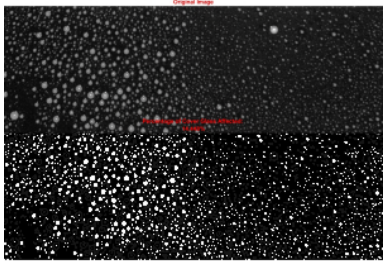
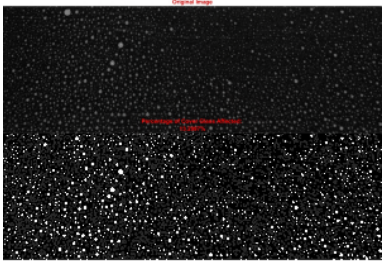
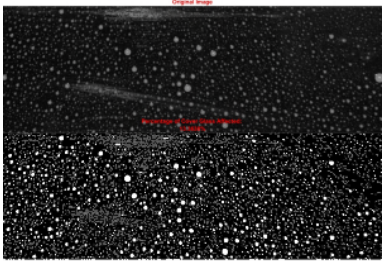
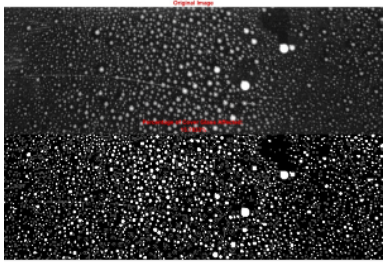
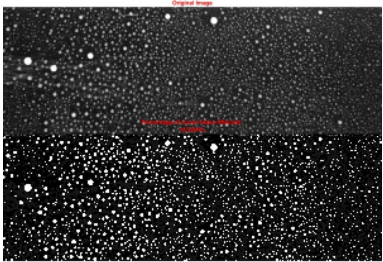
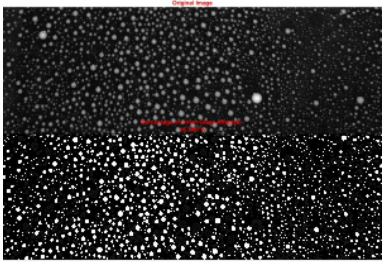
| Test 1  | Test 2  | Test 3  |
|---|---|---|
|    |    |    |
| 10.85%  | 7.45%   | 6.46%   |
| Test Set A  |   |   |
| Test 1  | Test 2  | Test 3  |
|    |    |    |
| 6.8%  | 8.4%  | 9.9%  |
| Test Set B  |   |   |
| Test 1  | Test 2  | Test 3  |
|  |  |  |
| 7.2%  | 7.84%   | 6.18%   |
| Test Set C  |   |   |
| Test 1  | Test 2  | Test 3  |
|  |  |  |
| 8.12%   | 10.45%  | 9.35%   |
| Test Set D  |   |   |
| Test 1  | Test 2  | Test 3  |



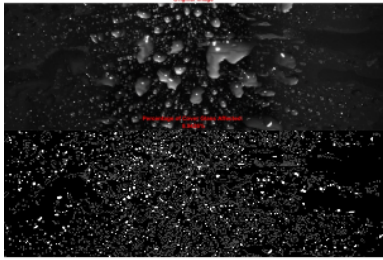
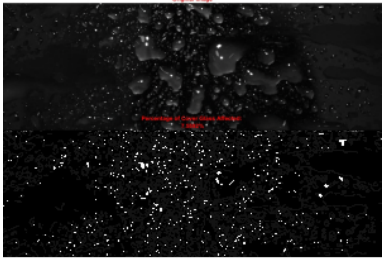
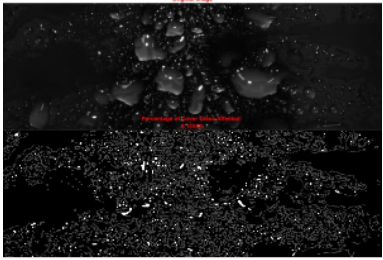
|   |   |   |
|---|---|---|
|  |  |  |
| 10.31%  | 10.57%  | 7.75%   |
| <b>Test Set E</b>   |   |   |
| <b>Test 1</b>   | <b>Test 2</b>   | <b>Test 3</b>   |
|  |  |  |
| 10.85%  | 7.45%   | 6.46%   |

## - LiDAR B

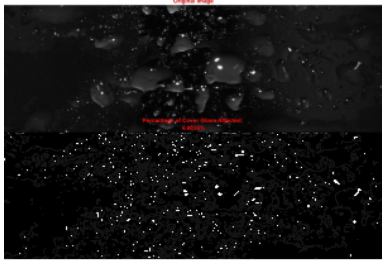
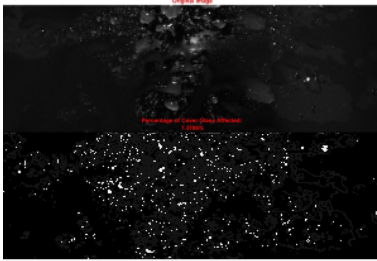
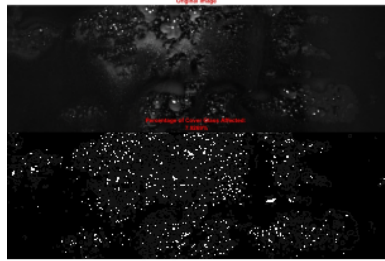
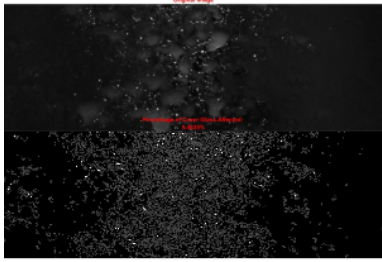
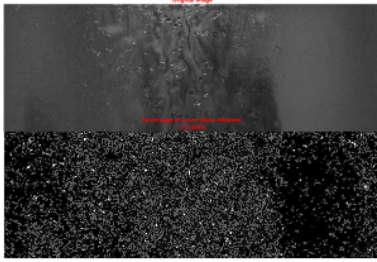
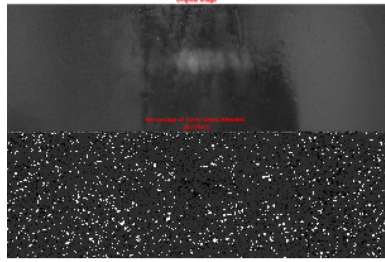
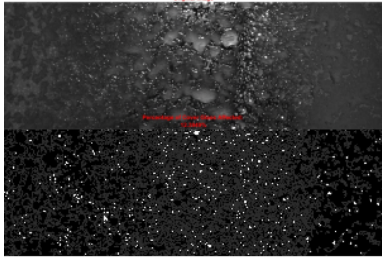
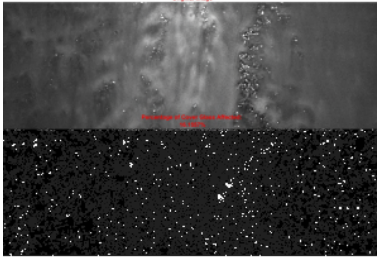
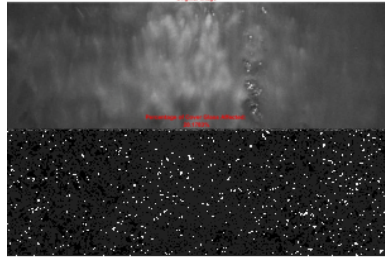
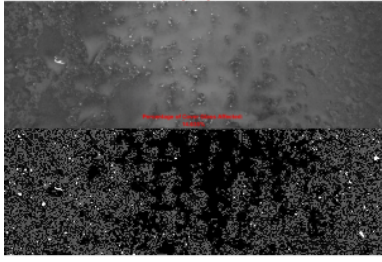
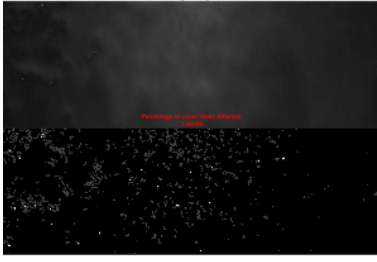
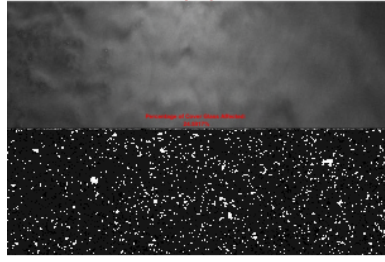
|   |   |   |
|---|---|---|
| <b>Test Set A</b>   |   |   |
| <b>Test 1</b>   | <b>Test 2</b>   | <b>Test 3</b>   |
|  |  |  |
| 13.79%  | 10.84%  | 9.64%   |
| <b>Test Set B</b>   |   |   |
| <b>Test 1</b>   | <b>Test 2</b>   | <b>Test 3</b>   |
|  |  |  |
| 13.89%  | 13.1%   | 11.1%   |
| <b>Test Set C</b>   |   |   |
| <b>Test 1</b>   | <b>Test 2</b>   | <b>Test 3</b>   |

|   |   |   |
|---|---|---|
|    |    |    |
| 13.36%  | 13.62%  | 14.96%  |
| <b>Test Set D</b>   |   |   |
| Test 1  | Test 2  | Test 3  |
|    |    |    |
| 14.45%  | 13.3%   | 13.36%  |
| <b>Test Set E</b>   |   |   |
| Test 1  | Test 2  | Test 3  |
|  |  |  |
| 15.78%  | 16.92%  | 16.4%   |

■ LiDAR C

|   |   |   |
|---|---|---|
| <b>Test Set A</b>   |   |   |
| Test 1  | Test 2  | Test 3  |
|  |  |  |
| 8.94%   | 7.56%   | 8.14%   |
| <b>Test Set B</b>   |   |   |
| Test 1  | Test 2  | Test 3  |



|   |   |   |
|---|---|---|
|    |    |    |
| 6.69%   | 7.38%   | 7.93%   |
| <b>Test Set C</b>   |   |   |
| Test 1  | Test 2  | Test 3  |
|    |    |    |
| 6.48%   | 14.14%  | 26.78%  |
| <b>Test Set D</b>   |   |   |
| Test 1  | Test 2  | Test 3  |
|  |  |  |
| 12.39%  | 16.16%  | 20.18%  |
| <b>Test Set E</b>   |   |   |
| Test 1  | Test 2  | Test 3  |
|  |  |  |
| 14.64%  | 1.59%   | 24.59%  |

